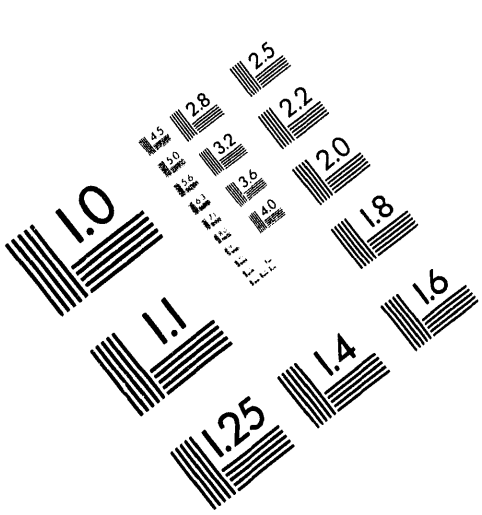

Association for Information and Image Management

1100 Wayne Avenue, Suite 1100
Silver Spring, Maryland 20910

301/587-8202

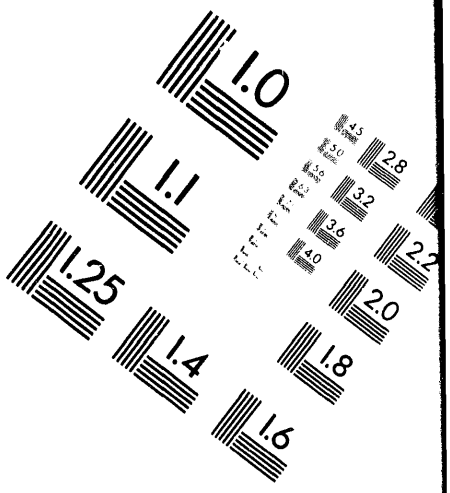

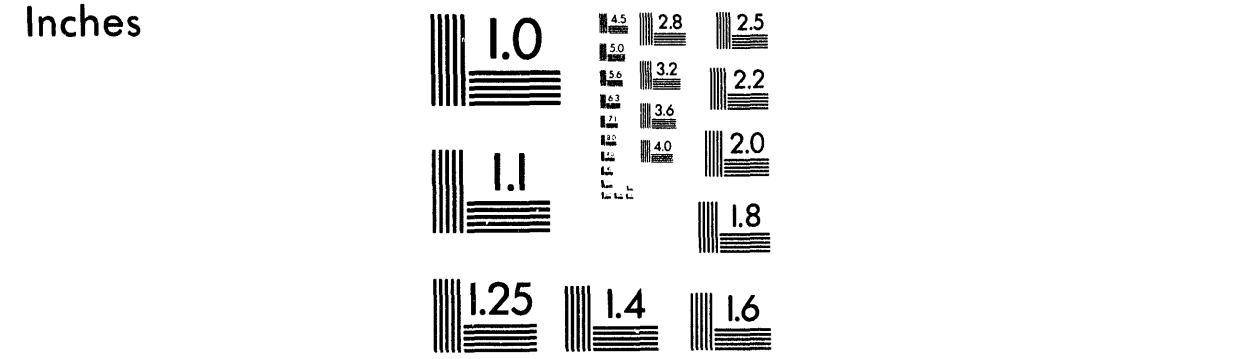

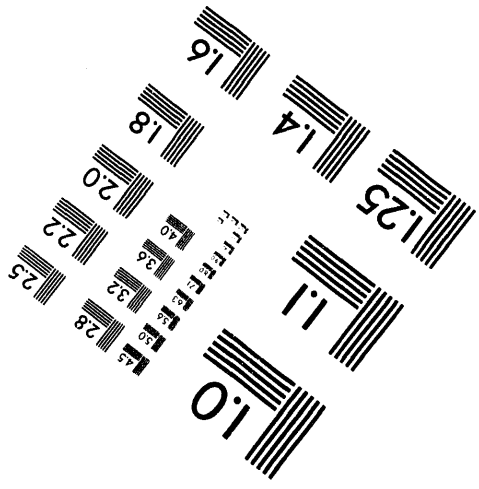

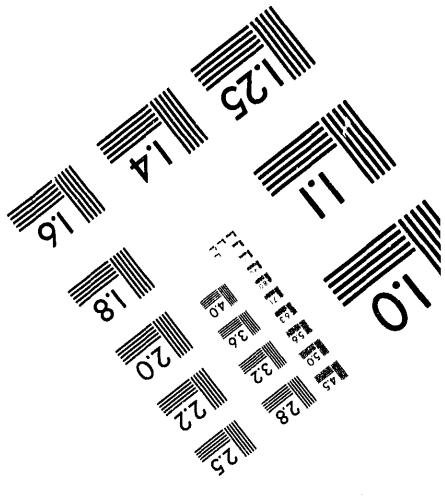

1 of 1

Key research issues in the pulsed fast-neutron analysis technique for cargo inspection

B. J. Micklich, C. L. Fink, and T. J. Yule

Technology Development Division
Argonne National Laboratory
Argonne, Illinois 60439 USA

ABSTRACT

Non-invasive inspection systems based on the use of fast neutrons are being studied for the inspection of large cargo containers. A key advantage of fast neutrons is their sensitivity to low-Z elements such as carbon, nitrogen, and oxygen, which are the primary constituents of explosives and narcotics. The high energy allows penetration of relatively large containers. The pulsed fast-neutron analysis (PFNA) technique is currently the baseline system. A workshop on the PFNA technique involving industrial, government, and university participants was held at Argonne National Laboratory in January 1994. The purpose of this workshop was to review the status of research on the key technical issues involved in PFNA, and to develop a list of those areas where additional modeling and/or experimentation were needed. The workshop also focused on development of a near-term experimental assessment program using existing prototypes and on development of a long-term test program at the Tacoma Testbed, where a PFNA prototype will be installed in 1995. A summary of conclusions reached at this workshop is presented. Results from analytic and Monte Carlo modeling of simplified PFNA systems are also presented.

1. INTRODUCTION

Fast-neutron interrogation techniques[1-4] are being studied for the detection of illicit substances in large cargo containers. In principle, fast-neutron based techniques can determine the densities of light elements such as carbon, nitrogen, and oxygen in a volume element. These elements are the primary constituents of many of the illicit substances one wishes to detect. In this paper, two techniques are discussed which are based on detecting gamma rays from fast-neutron interactions with the material being interrogated. The characteristic gamma rays allow one to determine the elemental densities. The two systems which are discussed below are being funded by the Advanced Research Projects Agency (ARPA). Other systems have been proposed, but will not be discussed here. Section 2 contains brief descriptions of the two systems. Section 3 contains a summary from a workshop hosted by Argonne National Laboratory in January 1994 to assess the status of and future directions for the two systems. Section 4 contains a discussion of modeling studies performed by Argonne for one of the systems.

2. DESCRIPTION OF THE TWO SYSTEMS

Both of the systems considered at the workshop were explicitly designed to inspect large cargo containers up to 2.4 m by 2.4 m by 12.2 m in volume for the presence of drugs. Each system uses a different technique to isolate a small volume of interest (voxel) within the larger container volume. Typical voxel sizes are $(10\ cm)^3$. Both systems detect essentially the same signatures from the elements located within the voxel. These signatures are combined in various ways to obtain a qualifier that is indicative of the presence or absence of an illicit substance. The requirement that the container be inspected in a relatively short period of time (typically 15 minutes) has a significant impact on system design.

In both of the nondestructive interrogation systems considered, the need to detect low-Z elements characteristic of drugs has led to the use of high-energy neutrons as the interrogation particle. This choice has the advantage that the signature gamma-rays produced by inelastic scattering or prompt gamma decay are also of high energy and thus have a relatively high transmission out of the cargo container to the gamma-ray detectors.

2.1 SAIC System

The system proposed[1] by SAIC produces approximately 8 MeV monoenergetic neutrons by using a tandem electrostatic accelerator to accelerate deuterons onto a deuterium gas target. The neutrons are collimated into a beam that is scanned vertically across the cargo container by a movable collimator. Scanning along the length of the container is accomplished by moving the container in a horizontal direction. The depth of the voxel within the container is obtained by performing a time-of-flight measurement between the accelerator pulse and the arrival of a gamma ray in NaI detectors located outside the container. An 8 MeV neutron has a velocity of 3.9 cm/ns, so the accelerator pulse width must be at most a few ns if the depth (thickness) of the voxel is to be restricted to about 10 cm. In addition, the coincidence system for the gamma-ray detectors must be better than a few nanoseconds.

The SAIC system uses the inelastic 4.44 MeV gamma ray from the first excited state in ^{12}C and the 6.13 MeV gamma ray from the second excited state in ^{16}O to generate a qualifier that indicates the presence or absence of drugs. Typically, drugs have a high carbon-to-oxygen ratio while other substances have a lower ratio.

The SAIC system has been under development for several years. It has completed the Phase 1 part of the ARPA program, which is Concept Design and Feasibility Testing. It is currently in the Prototype Design, Fabrication, and Laboratory Testing Phase, and will begin the Field Demonstration Phase at Tacoma in 1995.[5]

2.2 GAMMA-METRICS System

The GAMMA-METRICS system[2] uses 14-MeV neutrons produced by a (d,t) source. Collimators generate a fan-shaped neutron beam that illuminates a vertical slice of the cargo container. The horizontal position is varied by moving the cargo container. The vertical position and depth of the voxel are also defined by collimators, behind which are located the gamma-ray detectors. The GAMMA-METRICS system operates the neutron source in a pulsed mode with each pulse lasting several tens of microseconds. The inelastic 4.44 MeV and 6.13 MeV gamma rays from carbon and oxygen are detected during the active portion of each pulse. Prompt activation gamma rays characteristic of chlorine and nitrogen (PGNAA - Prompt Gamma Neutron Activation Analysis) and capture gamma rays from hydrogen (DGNAA - Delayed Gamma Neutron Activation Analysis) are detected between pulses. The GAMMA-METRICS system is currently in Phase 1 Concept Design and Feasibility Testing.

3. WORKSHOP SUMMARY

The objectives of the PFNA workshop which was held in January 1994 at Argonne National Laboratory were

(a) to review the status of the SAIC PFNA and the GAMMA-METRICS PFNA/PGNAA systems and to exchange scientific and technical information on these systems within a group consisting of participants from industry, federal agencies, government laboratories, and universities; and

(b) to review the modeling used in the PFNA system designs and to determine if additional modeling, computer codes, or cross-section data were needed.

Both SAIC and GAMMA-METRICS provided detailed overviews of their modeling efforts, of the current technical status of their programs, and of future efforts. The consensus of the participants was that the modeling efforts that have been performed are sufficient to determine the key engineering parameters of the two systems at the stage at which they are being tested. While there are uncertainties in some of the model parameters, the use of specific experimental measurements has reduced the effect of these uncertainties. Thus additional modeling is required only for fine-tuning system performance or to determine the system's range of capabilities. Some efforts in this regard are presented in Section 4 of this paper.

There was also a consensus that optimization of the prototype systems as well as the design of future systems would require some additional work in the areas of cross-section data and computer code development. There is considerable uncertainty in the cross-section data for certain reactions of interest. This is especially true in terms of the angular distributions of gamma rays emitted from oxygen and in the total neutron cross-section data for elements found in detectors such as iodine and germanium. A subcommittee met and determined a list of key measurements and evaluations that would be useful in optimizing system

performance and future designs. The emphasis in developing this list was on cross sections needed in drug detection, but there was also some interest expressed in extending the measurements to include cross-sections required in explosive detection.

In terms of computer codes there was agreement that faster Monte Carlo codes (especially involving complicated PFNA and PGNAA geometries) would be useful. The development of faster codes, implementing the codes on parallel processors, and porting to faster work stations were considered. Also, the availability of an adjoint capability in the Lawrence Livermore code COG[6] and an expanded adjoint capability in MCNP[7] would be useful.

4. ARGONNE MODELING STUDIES

While the results from analytic or computer simulations of PFNA systems are quite sensitive to the exact details of the source and detector characteristics, geometry, and assumed container contents, many basic physics questions can be addressed using simple models. These questions include the time and spatial dependencies and the dynamic range of the detected signals, and the effects of neutron and gamma ray scattering. In addition, modeling studies help to define a system's range of capabilities. This section describes both analytic and Monte Carlo studies which address these issues.

4.1 Analytic model for PFNA signal prediction

A simple geometry of a typical PFNA system of the type proposed by SAIC is shown in Figure 1. A short (~ 1-2 nsec) burst of collimated, monoenergetic neutrons is incident on the container. The neutrons interact with the material inside the container to create inelastic-scatter gamma rays. The minimum neutron energy required to excite inelastic levels is 4.44 MeV for carbon and 6.13 MeV for oxygen. For this type of system, incident energies are typically between 8 and 8.5 MeV. The gamma rays are observed by detectors arranged around the container. The point at which the gamma ray was created is determined by measuring the time between the source neutron burst and the time at which the gamma ray is detected. The interaction location is determined using the sum of the flight times of the neutron and gamma ray. An analytic representation of the expected signal can be obtained for any detector location by treating the container depth as a discrete variable z_i, and calculating the expected signal S_i at time t_i.

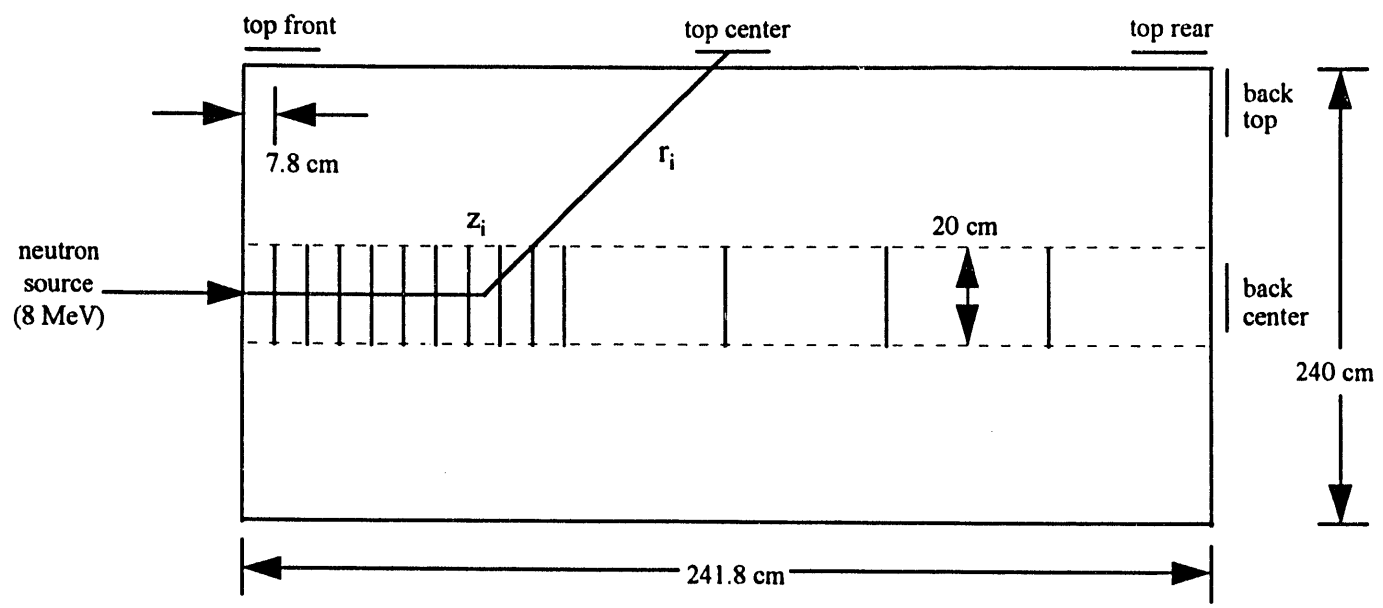

Figure 1. Schematic of the geometry of a typical Pulsed Fast-Neutron Analysis system (not drawn to scale), showing detector locations for the analytic model for PFNA signal prediction.

$$t_i = z_i/v_n + r_i/v_\gamma \qquad S_i = \phi_o \exp[-\lambda z_i]\,(N_t\sigma)\,(A_d/4\pi r_i^2)\exp[-\mu r_i] \qquad (1)$$

In these equations z_i is the depth at which the interaction occurs; r_i is the flight path length for the gamma ray to a given detector; v_n and v_γ are the neutron and gamma ray velocities, respectively; ϕ_o is the neutron flux at the container front face; λ is the attenuation constant for neutron flux; N_t is the number of target nuclei in a volume element; σ is the inelastic scatter cross section; A_d is the projected area of a detector; and μ is the gamma ray attenuation constant. The penetration depth is discretized into intervals 2 ns thick, which is 7.8 cm for an 8 MeV neutron (v_n =3.9 cm/ns). The container thickness in terms of flight time is 62 nsec. The attenuation constant λ, which characterizes the falloff of the inelastic scattering rate with depth, was determined from computer simulation and found to be approximately 0.049/cm for both the $^{12}C(n,n1)$ and $^{16}O(n,n2)$ reactions.

Figures 2 and 3 show $^{12}C(n,n1)$ gamma-ray signals calculated with this analytic model for detector locations on the top and at the back (Fig. 1) of a cargo container uniformly loaded with sugar at 0.5 g/cm^3. This corresponds to a heavily loaded container. Similar results are obtained for the $^{16}O(n,n2)$ gamma-ray signals. Several interesting points can be seen from these results.

1) All detectors, even those at the rear of the container, see the strongest signals at early times, and thus see more gamma rays originating from the front of the container than from the rear. This is because the inelastic-scatter gamma rays have longer mean free paths than the incident neutrons.

2) For detectors along the container top, the largest signal at early times (i.e., when the incident neutron pulse first enters the container) is seen by detectors near the front. Likewise, at middle times (when the incident neutrons pass through the center of the container) detectors in the middle see stronger signals than those closer to either the front or back, and at later times (when the incident neutron pulse reaches the rear of the container) detectors toward the back see stronger signals than those further forward.

3) For all detectors, the ratio of strongest to weakest gamma-ray signal is between 10 and 10^6. The ratio of strongest to weakest signal is largest for detectors near the front, since they have the shortest combined neutron plus gamma path for neutron interactions occurring near the front and the longest combined path for interactions occurring near the rear. This means that in a pulsed operating mode, all detectors will mainly be counting gammas which originate at the front of the container, and few gammas will be counted that come from the rear, so that little knowledge can be obtained about the contents in the back half of the container if the container is heavily loaded.

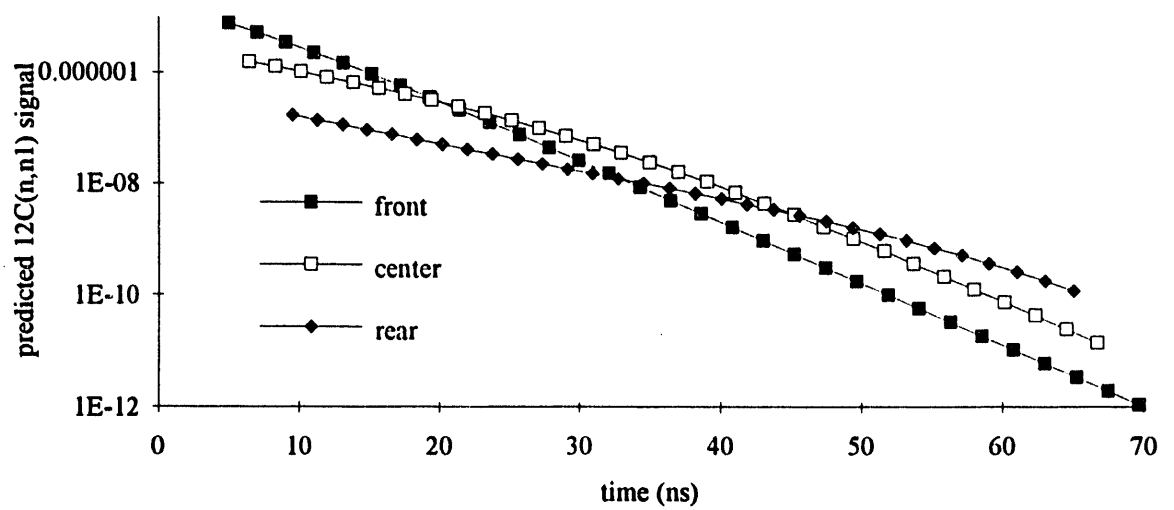

Figure 2. Analytic prediction of $^{12}C(n,n1)$ gamma-ray signal for detectors located at the front, center, and rear of the top surface of a cargo container containing a uniform loading of sugar with density 0.5 g/cm^3.

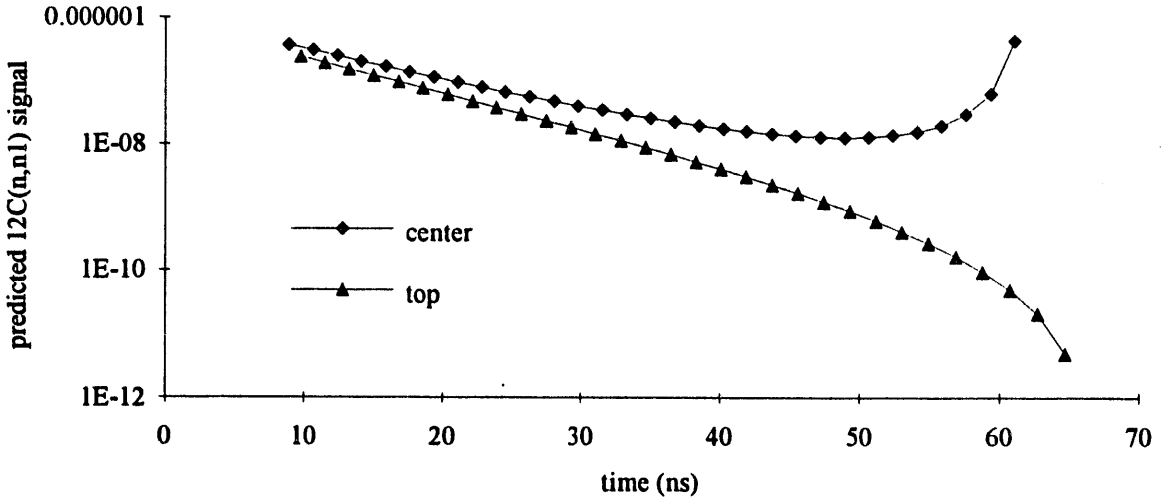

Figure 3. Analytic prediction of $^{12}C(n,n1)$ gamma-ray signal for detectors located at the top and center of the rear surface of a cargo container containing a uniform loading of sugar with density 0.5 g/cm^3.

4) The length of time over which gamma rays arrive at various detectors depends on the detector's position, because of the finite velocity of the gamma rays. Comparing two detectors at the front and rear of the container top, the front detector sees gammas arrive sooner and end later. Thus each detector will have a different time zero and bin width depending on its location. These parameters will vary depending on the location of the incident neutron beam, since they depend on the geometric arrangement of the gamma source and detector. This means that adding gamma-ray signals from several detectors to increase effective solid angle must be done carefully.

(5) For detectors at the rear of the container (Figure 3), the gamma signal increases at later times because of the solid angle factor. This occurs in this model because the detector is right at the back face; if it were located further behind the back face, the increase at later times would be reduced or, at large enough distances, disappear.

4.2 Monte Carlo model for PFNA signal prediction

Although the use of analytic models can yield much insight into the physics of an interrogation concept, subsequent analysis should treat more accurately the source and detector characteristics, physics of the transport and interaction processes, uncertainties and noise in the detected signal, and the procedures for data analysis and substance identification. Monte Carlo transport codes are ideal for this type of analysis since they combine the simplicity, flexibility, and power required to conduct investigations of basic physics questions surrounding candidate nuclear techniques. In addition, the range of capabilities of candidate systems can be assessed more easily, quickly, and inexpensively than with an experimental program.

The PFNA geometry described above was modeled with the radiation transport code MCNP[7] to estimate the signal at various detector locations for a uniform container loading of 0.5 g/cm^3 of sugar. For these models, variance reduction techniques such as exponential transform and weight window[8] are employed to adequately determine the neutron interaction and gamma-ray transport deep inside the container. A calculation of the gamma-ray signal from $^{12}C(n,n1)$ is shown in Figure 4, along with the analytic signal prediction discussed above. One can see that the MCNP simulation results show less attenuation as a function of time (distance into container) than those from the analytic prediction. This greater number of counts seen in the MCNP simulation is directly attributed to gamma rays produced by neutrons which have scattered away from their initial direction into the container. These gamma rays are created in regions off the beam axis, and thus do not follow the time-position correlation assumed in Equation 1. This can be directly shown by tabulating the gamma rays generated inside a 10-cm radius cylinder which is coaxial with the beam axis, and transporting these gamma rays to the detector in another MCNP simulation. The result is equivalent to the signal detected if one used collimated detectors to look only along the incident neutron beam axis. Figure 4 shows that the signal due to gamma rays generated inside this cylinder is close to the analytic signal prediction. Simi-

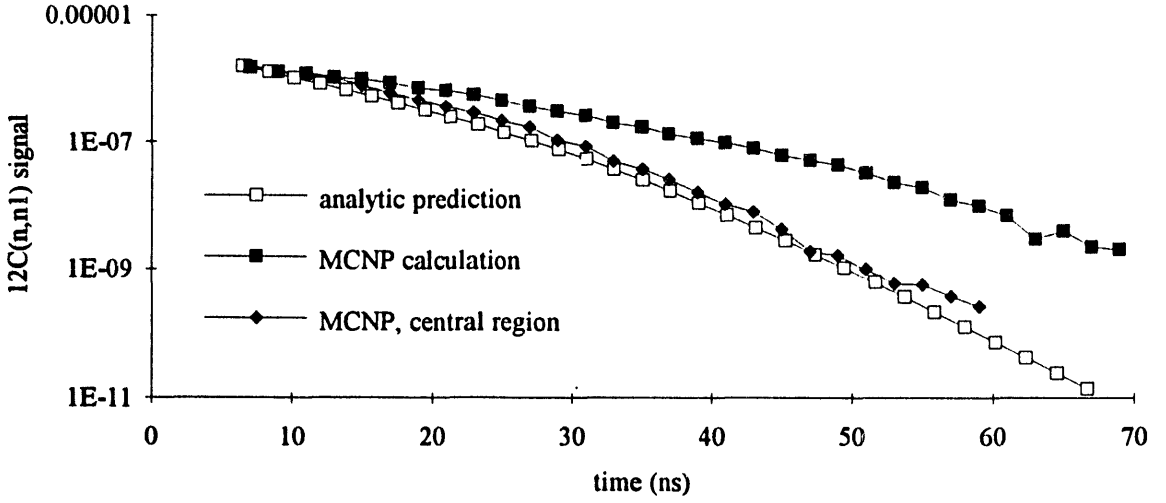

Figure 4. Comparison of predicted $^{12}C(n,n1)$ signal from analytic model vs. MCNP simulation for a detector located in the center of the top surface of a cargo container containing a uniform loading of sugar with density 0.5 g/cm^3.

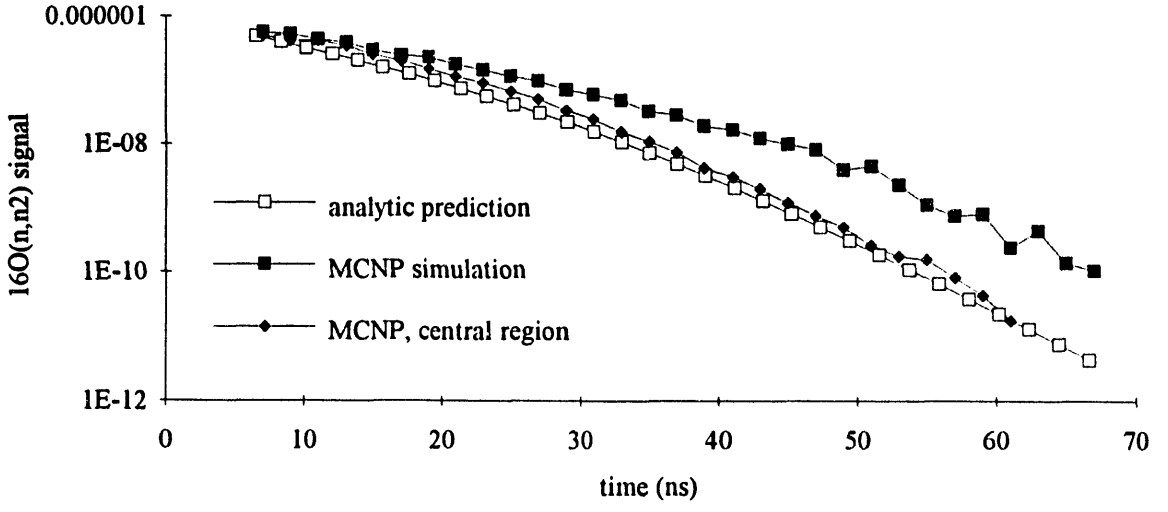

Figure 5. Comparison of predicted $^{16}O(n,n2)$ signal from analytic model vs. MCNP simulation for a detector located in the center of the top surface of a cargo container containing a uniform loading of sugar with density 0.5 g/cm^3.

lar results are seen in Figure 5 for the signal from $^{16}O(n,n2)$. In these figures, the scatter in the data at larger times is caused by worsening statistics in the Monte Carlo simulations.

Having determined the gamma-ray spectrum as a function of time for certain detector locations, we then need to extract information about elemental densities inside the container. Densities are unfolded from the simulated signal using the equations

$$n_c(t_i) = S_c(t_i) / \left[e^{-\lambda z_i} (V\sigma_c) \left(A_d / 4\pi r_i^2 \right) e^{-\mu_c r_i} \right] \quad \text{and} \quad n_o(t_i) = S_o(t_i) / \left[e^{-\lambda z_i} (V\sigma_o) \left(A_d / 4\pi r_i^2 \right) e^{-\mu_o r_i} \right] \tag{2}$$

This model is equivalent to using the inverse of the analytic signal prediction model above. This model assumes that gamma rays caused by scattered neutrons are unimportant (which is not necessarily a true assumption). To determine n_c and n_o we would have to know the details of the container contents, because we need to know λ, μ_c and μ_o. (where μ_c and μ_o. are the attenuation coefficients for the carbon and oxygen gamma rays, respectively) as functions of position throughout the container. It has been proposed to detect drug contraband using the fact that drugs are relatively rich in carbon and poor in oxygen compared to most substances. Thus detection based on the ratio of concentrations C/O (or C^2/O) has been suggested as a detection parameter. However, we can express the ratio n_c/n_o as

$$\frac{n_c}{n_o} = \frac{S_c(t_i)\cdot\sigma_o}{S_o(t_i)\cdot\sigma_c}\cdot e^{(\mu_c-\mu_o)r_i} \tag{3}$$

which still requires knowledge of μ_c and μ_o. Figure 6 shows this detection parameter as a function of depth for the MCNP simulation discussed above (sugar at 0.5 g/cm^3), using the appropriate correction for the gamma attenuation. These results are based on simulation results for the top center detector (Figure 1). The true C/O ratio is unity for this material loading.

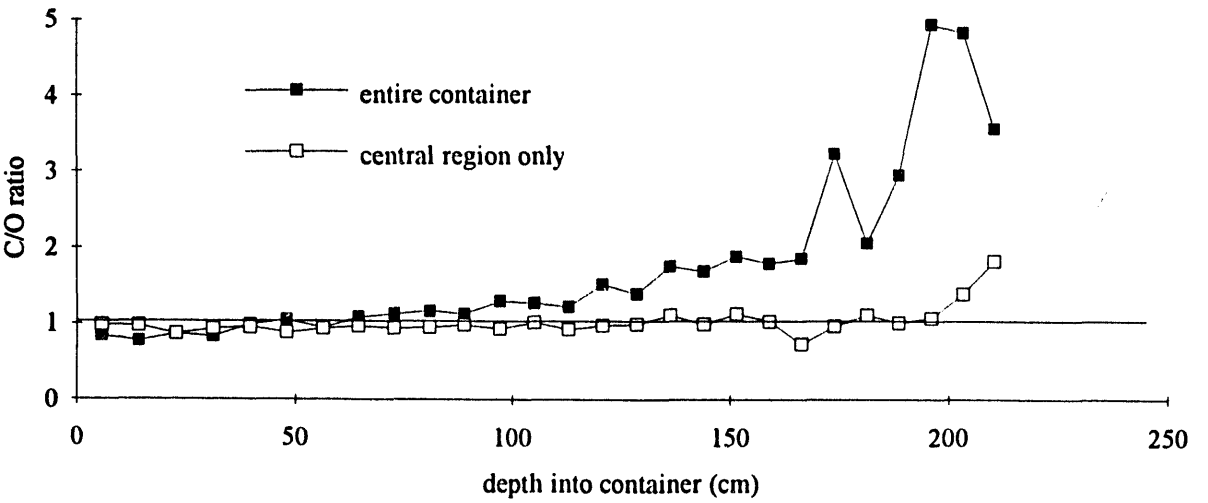

Figure 6. Variation of detection parameter C/O with depth into container (0.5 g/cm^3 sugar) from MCNP simulation (determined using results for top center detector).

The increase in C/O with depth for uncollimated detectors is due to the detection of gamma rays produced by neutrons which have scattered away from the incident beam axis. This scattering effect is stronger in carbon than in oxygen because the lower threshold energy for inelastic events in carbon allows neutrons to scatter more times before losing enough energy to pass beneath the threshold. The ratio C/O departs most significantly from unity in the back half of the container; thus this technique may be useful only in the front half for this example, making it necessary to irradiate from both sides.

4.3 Study of effects of hydrogen in scattering material

Hydrogen is often thought to be bad for fast-neutron interrogation systems because of its well-known moderating properties. However, in PFNA-type systems water can perhaps be of benefit in the sense that neutrons which are elastically scattered out of the incident beam are reduced quickly in energy beneath the threshold for inelastic scattering. This would reduce the number of inelastic-scatter gamma rays originating from off-axis regions. To investigate these effects, simulations were run to determine the space and time dependence of inelastic gamma-ray generation in a 2.4 m cubic assembly of materials containing hydrogen (sugar, polyethylene) and a similar material without hydrogen (graphite). The sugar is taken to have density 0.5 g/cm^3 as previously, and the other materials have their densities chosen so that the neutron mean free path is the same in all three materials.

Thus the penetration of incident uncollided neutrons is the same in all three cases. The material parameters are given in Table 1. The $^{12}C(n,n1)$ inelastic scatter rate is determined in a spatial grid having concentric cylinders with radii in 10 cm increments and axial divisions every 7.8 cm (2 ns flight time for 8 MeV neutrons), and over time bins which are 2 ns wide. The results were tabulated to give (i) the gamma-ray source strength along the incident beam axis and (ii) profiles of the gamma-ray source strength as a function of axial and radial position for various time slices. The results for polyethylene are identical to those for sugar, so only the results for sugar will be given.

Table 1. Material parameters for investigation of effects of hydrogen on PFNA signal generation.

material	mass density (g/cm^3)	atom density ($10^{24}/cm^3$)	H atom density	C atom density	O atom density
graphite	0.5238	0.02626	-	0.02626	-
sugar $(CH_2O)_x$	0.5	0.04012	0.02006	0.01003	0.01003
polyethylene (CH_2)	0.2788	0.03591	0.02394	0.01197	-

Figure 7 shows the inelastic scattering rate due to uncollided neutrons as a function of position (equivalent to time) for graphite and sugar media. The inelastic scattering rate is the same near the front face, but the $^{12}C(n,n1)$ rate in sugar is 80% of that in graphite after 50 cm depth, decreasing to 75% at about 125 cm and about 73% at the rear face. Thus there would be no appreciable reduction in signal strength in a hydrogenous versus non-hydrogenous medium.

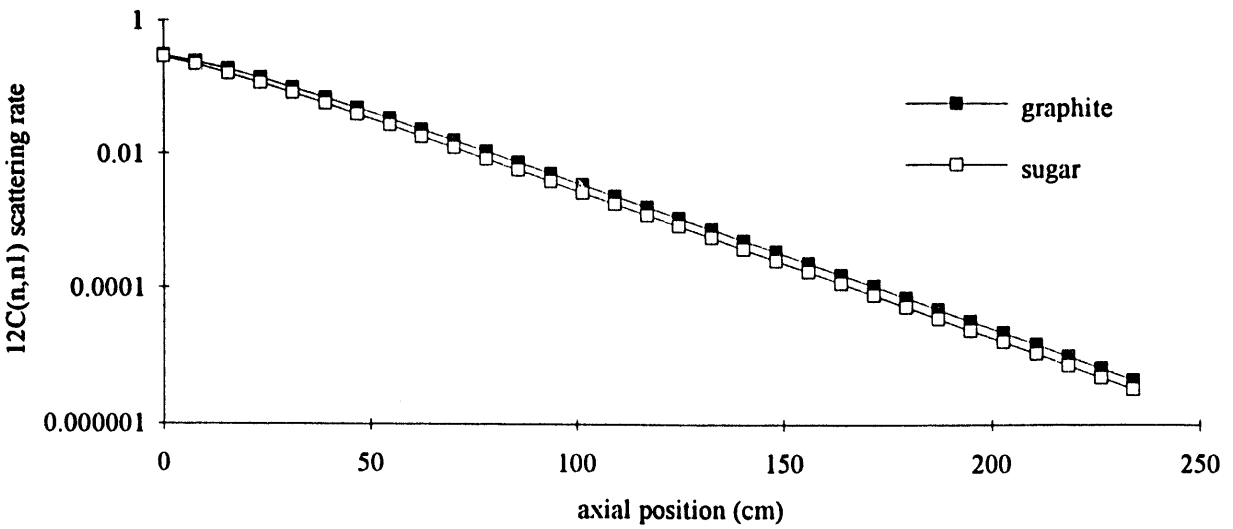

Figure 7. $^{12}C(n,n1)$ inelastic scattering rate due to uncollided neutrons for 8 MeV neutrons incident on graphite and sugar assemblies.

Figures 8 and 9 show radial and axial profiles of the $^{12}C(n,n1)$ inelastic scattering rate in the sugar and graphite cubes at various times [t = 30 ns corresponds to uncollided incident neutrons halfway through the cube]. These profiles have been normalized so that the reaction rate per unit volume due to uncollided neutrons is 1. One can see how the neutrons which have scattered off the beam axis create gamma rays throughout the entire cube, and how the relative number of these gamma rays increases as the uncollided incident neutrons penetrate into the cube. The relative number of gammas due to neutrons which have elastically scattered away from the incident beam axis is much smaller in the sugar medium, due to the moderating effect of the hydrogen. For example, at 30 ns the fraction of gammas created by the uncollided incident neutrons is 0.069 in the graphite cube and 0.185 in the sugar cube. At 50 ns, these fractions are 0.0062 and 0.049.

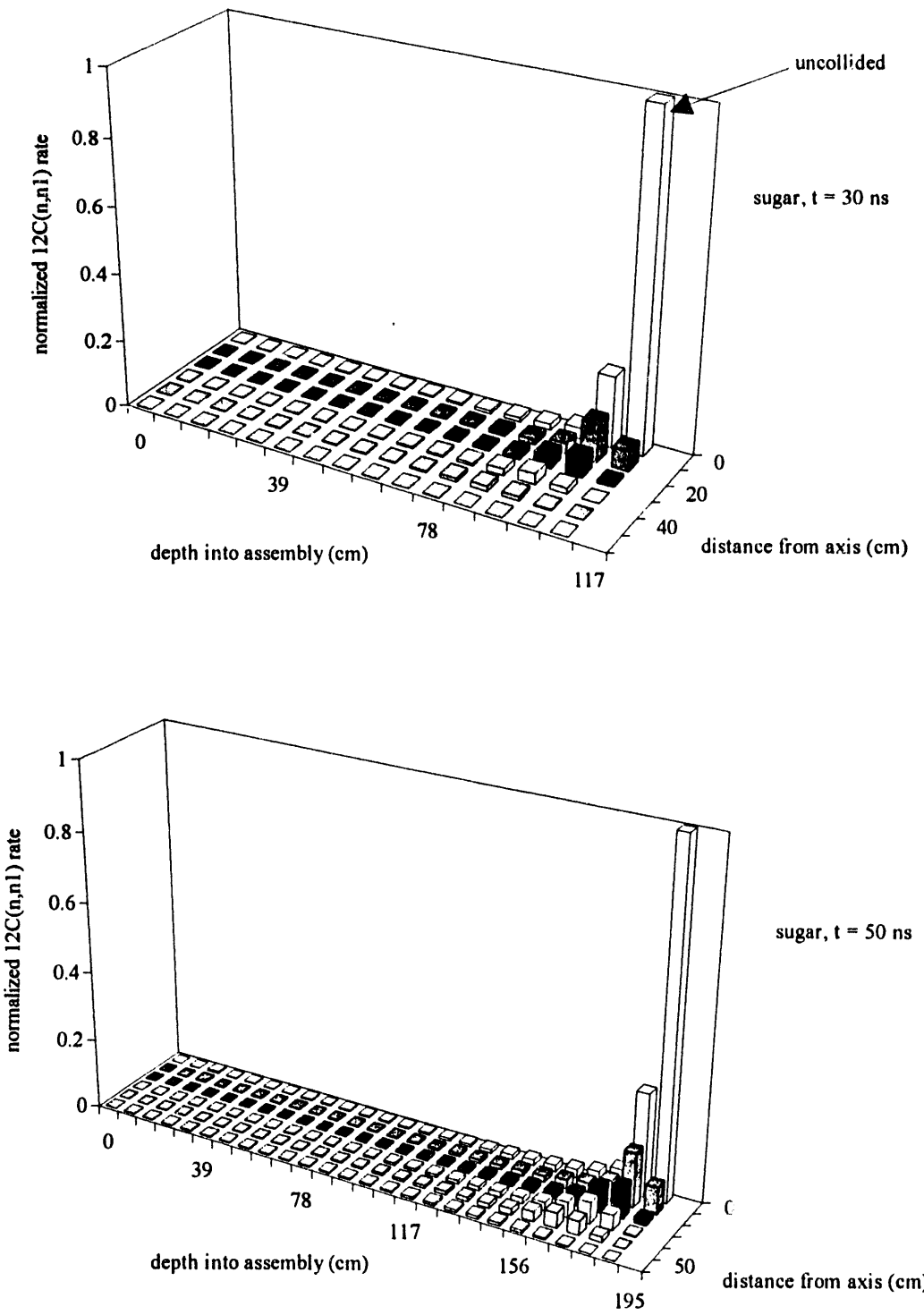

Figure 8. $^{12}C(n,n1)$ reaction rate in sugar assembly as a function of space and time. The $^{12}C(n,n1)$ reaction rate is normalized so that the reaction rate per unit volume in the spatial grid containing the incident neutron pulse is 1. The figure shows the increase of gamma rays created by scattered neutrons as the incident neutrons penetrate further into the assembly.

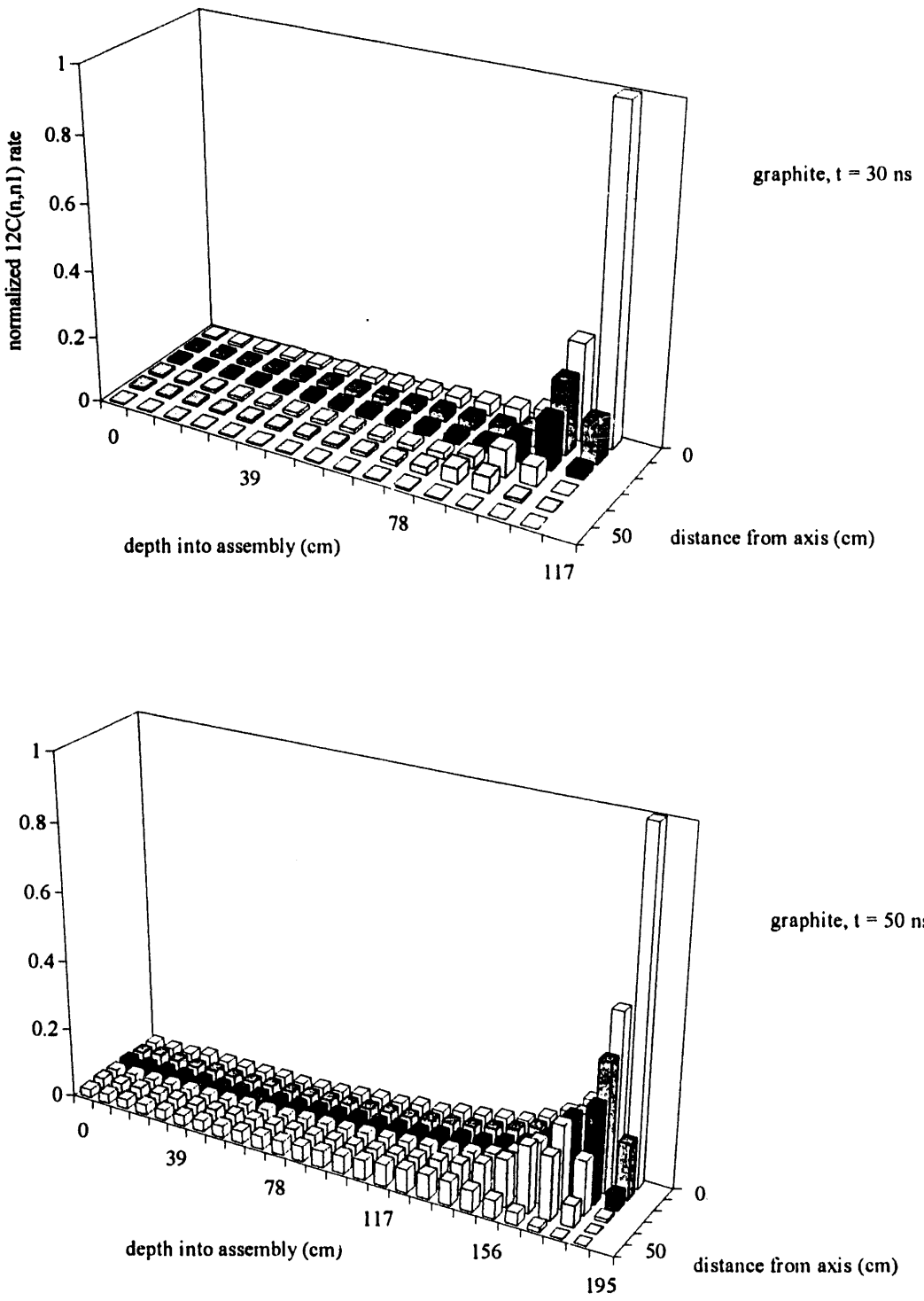

Figure 9. $^{12}C(n,n1)$ reaction rate as a function of space and time in a graphite assembly. The $^{12}C(n,n1)$ reaction rate is normalized so that the reaction rate per unit volume in the spatial grid containing the incident neutron pulse is 1. The increase of gamma rays due to scattered neutrons is much greater than in the sugar assembly.

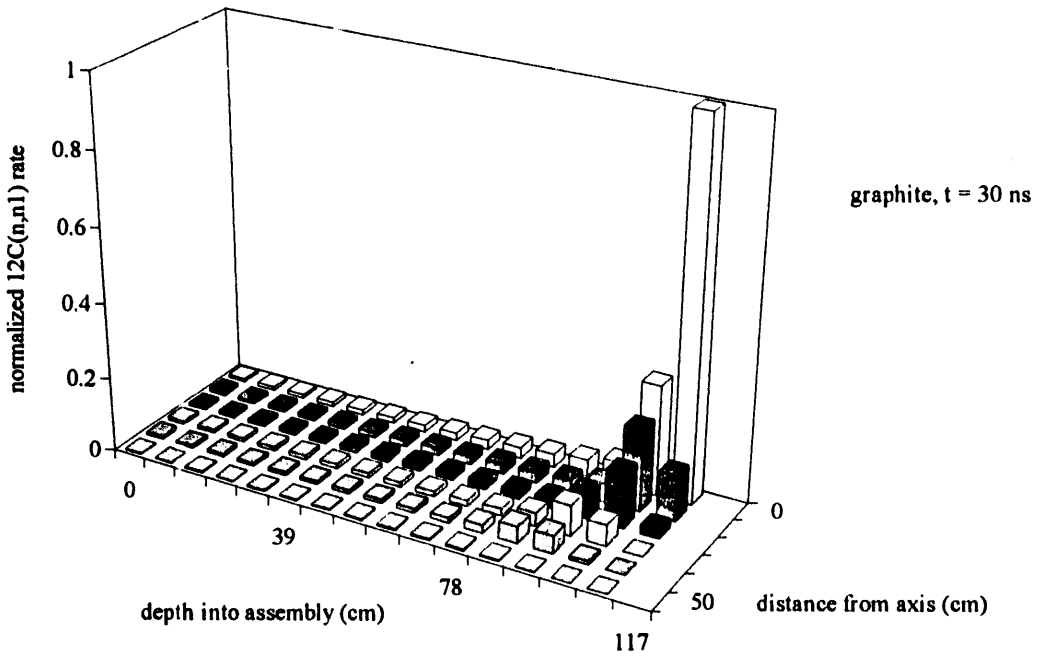

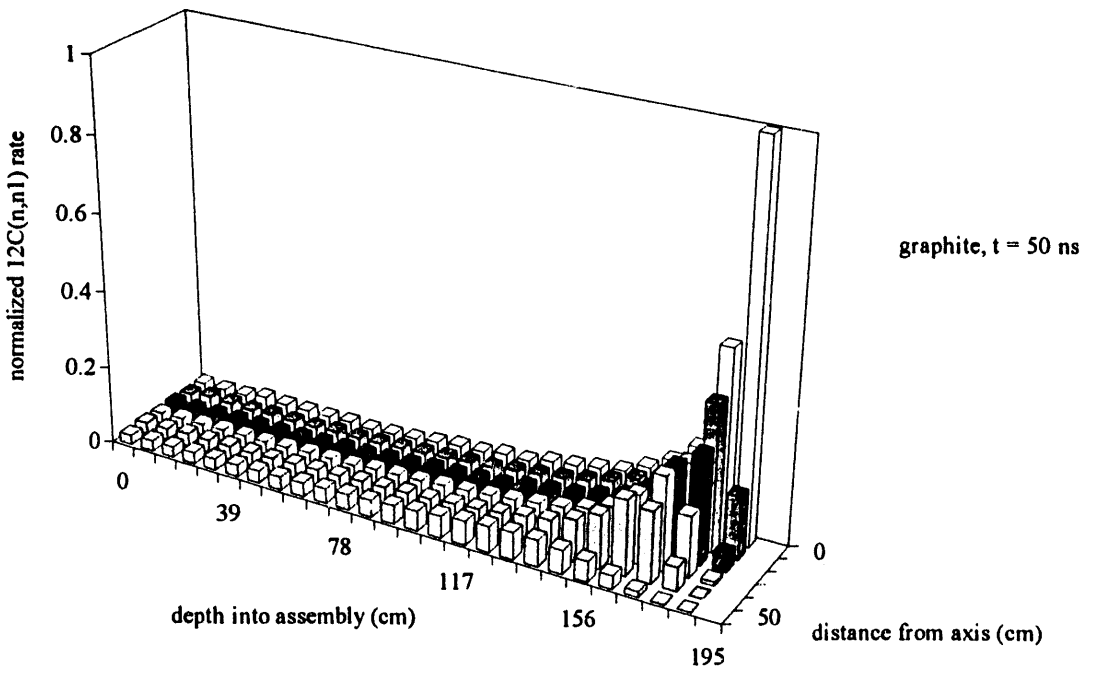

Figure 9. $^{12}C(n,n1)$ reaction rate as a function of space and time in a graphite assembly. The $^{12}C(n,n1)$ reaction rate is normalized so that the reaction rate per unit volume in the spatial grid containing the incident neutron pulse is 1. The increase of gamma rays due to scattered neutrons is much greater than in the sugar assembly.

Combining the results from Figures 7-9 lead to two important conclusions. (1) The gamma source due to inelastic scatter of uncollided incident neutrons is not much smaller in a hydrogenous material having the same mean free path for incident neutrons as a similar but non-hydrogenous material. (2) The signal derived from the hydrogenous material will be "cleaner" in the sense that a higher fraction of the gammas detected will be due to interactions within the volume of interest rather than those occurring elsewhere in the volume. These results again point out the utility of irradiating heavily loaded cargo containers from both sides during inspection, with each irradiation examining one-half of the container depth, so that one minimizes the effects of neutron scattering.

5. CONCLUDING REMARKS

In order to determine the applicability and limitations of the PFNA technique based on physics considerations, it is necessary to perform both analytic and Monte Carlo transport code modeling studies. The effect of neutron scattering can be significant for particular geometries and cargo loadings. This places a limitation on the minimum amount of illicit substance which can be detected in a cargo container. Of course, other limitations will be introduced by systems issues such as accelerator parameters, detector efficiency, statistics, and data processing time. We are also examining these system issues in conjunction with the physics studies presented here.

6. ACKNOWLEDGMENTS

This work was sponsored by the Counterdrug Technology Assessment Center of the U. S. Office of National Drug Control Policy under contract number 6-CO-160-00-195.

7. REFERENCES

1. D. R. Brown, R Loveman, J. Bendahan, M. Schulze, "Cargo Inspection System Based on Pulsed Fast-Neutron Analysis," *Proc. Int'l Symp. on Contraband And Cargo Inspection Technology*, pp. 235-241, Washington, DC (Oct. 1992).
2. M. J. Hurwitz, R. C. Smith, W. P. Noronha, and K.-C. Tran, "Detection of Illicit Drugs in Cargo Containers Using Pulsed Fast Neutron Analysis," *Proc. Int'l Symp. on Contraband and Cargo Inspection Technology*, pp. 29-36, Washington, DC (Oct. 1992).
3. G. Vourvopolous, F. J. Schulz, and J. Kehayias, "A Pulsed Fast-Thermal Neutron Interrogation System," *Proc. 1st Int'l Symp. on Explosive Detection Technology*," DOT/FAA/CT-92/11, pp. 104-115, Atlantic City, NJ (May 1992).
4. E. Rhodes and C. W. Peters, "APSTNG: Neutron Interrogation for Detection of Drugs and Other Contraband," *Proc. Int'l Symp. on Contraband And Cargo Inspection Technology*, pp. 37-44, Washington, DC (Oct. 1992).
5. R. F. Reiter, R. Volberding, A. J. Johnson, "DARPA Cargo Container Inspection Technology Test Bed Program," *Proc. Int'l Symp. on Contraband And Cargo Inspection Technology*, pp. 227-234, Washington, DC (Oct. 1992).
6. T. P. Wilcox and E. M. Lent, "COG, A Particle Transport Code Designed to Solve the Boltzmann Equation for Deep-Penetration (Shielding) Problems, LLNL Report M-221-1.
7. J. Briesemeister, ed., "MCNP - A Generalized Monte Carlo Code for Neutron and Photon Transport, Version 3A," LA-7396-M, Rev. 2, Los Alamos National Laboratory (Sept. 1986).
8. T. Booth, "A Sample Problem for Variance Reduction in MCNP," LA-10363-MS, Los Alamos National Laboratory (Oct. 1985).

DISCLAIMER

DATE
FILMED
8/25/94
END